18. Greenstein, G. & Hartke, G. J. Pulselike character of blackbody radiation from neutron stars. *Astrophys. J.* **271,** 283–293 (1983).
19. Pavlov, G. G., Zavlin, V., Trümper, J. & Neuhäuser, R. Multiwavelength observations of isolated neutron stars as a tool to prove the properties of their surfaces. *Astrophys. J. Lett.* **472,** L33–L36 (1996).
20. Holtzman, J. A. *et al*. The photometric performance and calibration of WFPC2. *Pub. Astron. Soc. Pacif.* **107,** 1065–1093 (1995).
21. Fruchter, A. S. & Hook, R. N. in *The Hubble Space Telescope and the High Redshift Universe* (eds Tanvir, N. R., Salamanca, A. & Wall, J. V.) (World Scientific, Singapore, 1997).

Acknowledgements. We thank A. M. Watson for performing the bulk of the image reduction, and J. Holtzman for peparing and providing the delta dark and superdark frames necessary for our data; we also thank them both for their time and patience in the discussion of data reduction issues. We acknowledge useful discussions with P. An, J. Lattimer and R. Neuhäuser.

Correspondence and requests for materials should be addressed to F.M.W. (e-mail: fwalter@astro.sunysb.edu).

A general boundary condition for liquid flow at solid surfaces

Peter A. Thompson* & Sandra M. Troian†

** The Celerity Group, 20 Nassau Street, Suite 209, Princeton, New Jersey 08542, USA*
† Department of Chemical Engineering, Princeton University, Princeton, New Jersey 08544, USA

Modelling fluid flows past a surface is a general problem in science and engineering, and requires some assumption about the nature of the fluid motion (the boundary condition) at the solid interface. One of the simplest boundary conditions is the no-slip condition[1,2], which dictates that a liquid element adjacent to the surface assumes the velocity of the surface. Although this condition has been remarkably successful in reproducing the characteristics of many types of flow, there exist situations in which it leads to singular or unrealistic behaviour—for example, the spreading of a liquid on a solid substrate[3–8], corner flow[9,10] and the extrusion of polymer melts from a capillary tube[11–13]. Numerous boundary conditions that allow for finite slip at the solid interface have been used to rectify these difficulties[4,5,11,13,14]. But these phenomenological models fail to provide a universal picture of the momentum transport that occurs at liquid/solid interfaces. Here we present results from molecular dynamics simulations of newtonian liquids under shear which indicate that there exists a general nonlinear relationship between the amount of slip and the local shear rate at a solid surface. The boundary condition is controlled by the extent to which the liquid 'feels' corrugations in the surface energy of the solid (owing in the present case to the atomic close-packing). Our generalized boundary condition allows us to relate the degree of slip to the underlying static properties and dynamic interactions of the walls and the fluid.

During the past decade molecular dynamics simulations have emerged as a powerful tool for probing the microscopic behaviour of liquids at interfaces (ref. 15, and references therein). Studies have demonstrated how solids induce order in adjacent liquids and how this order, in turn, controls the amount of momentum transfer[16]. The no-slip condition has been shown to be just one of many allowable flow boundary conditions ranging from pure slip to multi-layer locking. The degree of slip at the boundary depends on a number of interfacial parameters including the strength of the liquid–solid coupling, the thermal roughness of the interface, and the commensurability of wall and liquid densities[16]. These findings have led to a new understanding of stick-slip phenomena in boundary lubrication[17] and have revealed the sensitivity of liquid spreading to microstructure at the liquid/solid interface[7,8]. Earlier work[16] investigated flows in a regime for which the degree of slip was independent of local shear rate $\dot{\gamma}$. This regime is described by the well-known linear Navier boundary condition[1] in which $\Delta V = L_s\dot{\gamma}$, where ΔV is the velocity difference between the solid and adjacent liquid, and L_s is a constant slip length. Here we examine the

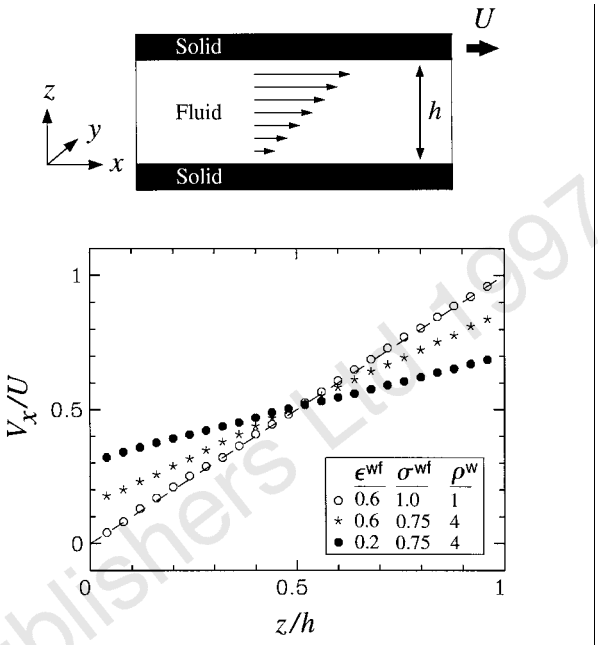

Figure 1 Steady-state flow profiles and schematic of the Couette flow geometry. The Couette cell measured $12.51\sigma \times 7.22\sigma \times h$ where h varied from 16.71σ to 24.57σ. The number of fluid molecules ranged from 1,152 to 1,728, respectively. The $\hat{\mathbf{x}}$-direction of the cell is aligned along the $[11\bar{2}]$ orientation of the face-centred cubic lattice comprising the wall, and periodic boundary conditions are imposed along $\hat{\mathbf{x}}$ and $\hat{\mathbf{y}}$. The flow profiles were obtained for systems with $U = 1.0\sigma\tau^{-1}$, $h = 24.57\sigma$, and walls characterized by the indicated density and Lennard–Jones parameters. Values for ϵ^{wf}, σ^{wf} and ρ^{w} (see text) are in units of ϵ, σ and ρ, respectively. Following an equilibration period of $\sim 100\tau$, the profiles were computed by averaging the instantaneous particle velocities within bins of width $\sim 1\sigma$ spanning the distance between the two walls. The duration of the averaging varied from 250τ to $7{,}000\tau$ depending on the signal-to-noise ratio. Accurate resolution of flows with $\dot{\gamma} < 0.01\tau^{-1}$ typically required $>2{,}500\tau$ of averaging. The dashed line indicates Couette flow with a no-slip boundary condition.

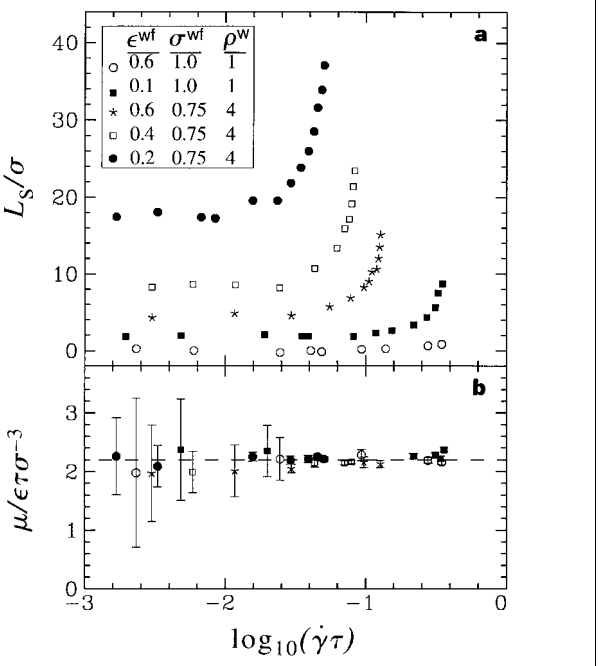

Figure 2 Variation of the slip length L_s (panel **a**) and viscosity μ (panel **b**) as a function of shear rate for systems with the indicated interfacial properties. L_s was computed from the definition $L_s = \Delta V_x/\dot{\gamma}$, which for Couette flow reduces to $(U/\dot{\gamma} - h)/2$: μ was computed from the relation $\mu = P_{zx}/\dot{\gamma}$, where P_{zx} is the zx-component of the microscopic stress tensor averaged across the cell[19].

boundary condition over a much wider range of shear rates which reveals a nonlinear relationship between L_s and $\dot{\gamma}$.

Our molecular dynamics simulations model a simple liquid undergoing planar shear in a Couette cell as shown in Fig. 1. Each wall of the cell consists of N_w atoms forming two (111) planes of a face-centred cubic lattice. N_w ranges from 144 to 576 depending on the wall density, ρ^w. The liquid is treated as an isothermal ensemble of spherical molecules. Molecules separated by a distance r interact through a shifted Lennard–Jones 6–12 potential:

$$V^{LJ}(r) = 4\epsilon\left[\left(\frac{\sigma}{r}\right)^{12} - \left(\frac{\sigma}{r}\right)^{6} - \left(\frac{\sigma}{r_c}\right)^{12} + \left(\frac{\sigma}{r_c}\right)^{6}\right] \quad (1)$$

where ϵ and σ are characteristic energy and length scales, and the potential is zero for $r > r_c = 2.2\sigma$. The wall–fluid interaction is also modelled with a truncated Lennard–Jones potential with energy and length scales ϵ^{wf} and σ^{wf}, respectively, and cut-off r_c. Similar systems have been widely used to investigate a variety of bulk and interfacial flows[15].

The equilibrium state of the fluid is a well-defined liquid phase characterized by number density $\rho = 0.81\sigma^{-3}$ and temperature $T = 1.1k_B/\epsilon$. Constant temperature is maintained by weakly coupling the particle dynamics to a thermal reservoir through the addition of Langevin noise and frictional terms to the equations of motion[7,8,16–18]. Good thermal coupling obviates the need for the noise and frictional terms in the $\hat{\mathbf{x}}$ and $\hat{\mathbf{z}}$ directions[16,18]. The resulting equation of motion for the y degree of freedom of the ith molecule of mass m is

$$m\ddot{y}_i = \sum_{j\neq i} \partial V^{LJ} \Big/ \partial y_i - m\Gamma\dot{y}_i + \eta_i \quad (2)$$

where $\Sigma_{j\neq i}$ denotes a sum over all interactions with i, Γ is a friction constant that controls the rate of heat exchange with the reservoir, and η_i is a gaussian distributed random force with zero mean and variance $2mk_BT\Gamma$. Efficient temperature control with minimal effect on particle dynamics was achieved with $\Gamma = 1.0\tau^{-1}$, where $\tau = (m\sigma^2/\epsilon)^{1/2}$ is the characteristic time of the Lennard–Jones potential. The equations of motion are integrated using a fifth-order Gear predictor–corrector algorithm[19] with a time step $\Delta t = 0.005\tau$.

The simulations produce steady-state velocity fields as shown in Fig. 1. The flows were induced by translating the upper wall with velocity U in the $\hat{\mathbf{x}}$ direction. The profiles recover the expected flow behaviour from continuum hydrodynamics with boundary conditions involving varying degrees of slip. For the system with $\rho^w/\rho = 1$ and $\epsilon^{wf}/\epsilon = 0.6$, $\Delta V_x/U = 0$ and the no-slip condition is obeyed exactly. For larger ρ^w or smaller ϵ^{wf}, slip is evident. This variation with wall properties is consistent with that reported earlier[16]—namely, the amount of momentum transfer at the wall/fluid interface decreases as the relative surface energy corrugation of the wall decreases. The corrugation is maximized when the wall and fluid densities are commensurate ($\rho^w = \rho$) and the strength of the wall–fluid coupling ϵ^{wf} is large. In this case, there is efficient momentum transfer and the resulting flow is consistent with a no-slip, or in extreme cases, a "stick" boundary condition[16]. For incommensurate densities or smaller couplings, the corrugation is weaker and interfacial slip develops.

We now consider how the fluid responds to variations in the wall speed U for five different sets of interfacial parameters (ϵ^{wf}, σ^{wf} and ρ^w). To generalize the analysis, the results are expressed in terms of the shear rate $\dot{\gamma}$ within the fluid measured directly from the computed linear velocity profiles as in Fig. 1. Note that the bulk viscosity μ of the fluid is a constant over the entire range of shear rates (Fig. 2b) indicating the bulk fluid remains newtonian. Based on previous investigations of shear-induced ordering in simple fluids, non-newtonian response of the bulk fluid is expected for $\dot{\gamma} \geq 2\tau^{-1}$ (ref. 20).

The variation in L_s as a function of $\dot{\gamma}$ is shown in Fig. 2a. The data

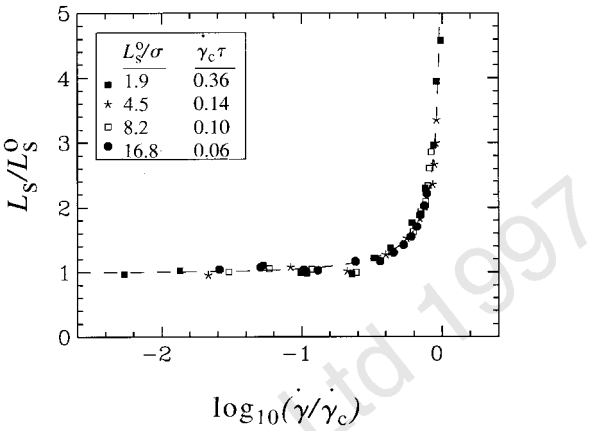

Figure 3 Master curve describing the flow boundary condition. The data is the same as that shown in Fig. 2a with L_s and $\dot{\gamma}$ scaled by the indicated values of L_s^o and $\dot{\gamma}_c$. The dashed line represents $L_s = L_s^o(1 - \dot{\gamma}/\dot{\gamma}_c)^{-1/2}$.

reveal several significant features. At sufficiently low $\dot{\gamma}$, the boundary condition is consistent with the Navier model. In this regime, the slip length equals its limiting value L_s^o which ranges from zero to $\sim 17\sigma$ for the interfacial parameters chosen. In general, the amount of slip increases with decreasing surface energy corrugation. The latter was achieved by either decreasing the wall–fluid coupling ϵ^{wf} or increasing the wall density ρ^w. At higher shear rates, the Navier condition breaks down as the slip length increases rapidly with $\dot{\gamma}$. Surprisingly, the boundary condition is nonlinear even though the liquid is still newtonian. In fact the slip length appears to diverge as the shear rate approaches a critical value $\dot{\gamma}_c$. This value depends on the surface energy corrugation: as the corrugation decreases, so too does $\dot{\gamma}_c$. We note that the values for $\dot{\gamma}_c$ shown in Fig. 2 are of the same magnitude as the shear rates previously found in molecular dynamics studies of low capillary number flows[7,8].

The functional behaviour for L_s suggests a universal boundary condition at a solid–liquid interface. Scaling L_s by its asymptotic limiting value L_s^o and $\dot{\gamma}$ by its critical value $\dot{\gamma}_c$ collapses the data onto the curve shown in Fig. 3. This curve is well described by the form $L_s = L_s^o(1 - \dot{\gamma}/\dot{\gamma})^{-\alpha}$ where the dashed line represents the value $\alpha = 1/2$. This behaviour suggests that close to a critical shear rate the boundary condition can significantly affect flow behaviour at macroscopic distances from the wall, an experimental observation repeatedly seen in many polymeric systems[21]. Such significant slip is not easily recoverable in the phenomenological models presented to date. It also suggests that for flows in the vicinity of $\dot{\gamma}_c$ small changes in the surface properties can lead to large fluctuations in the apparent boundary condition.

Given the remarkable collapse of the data, one would like to understand what causes L_s to diverge at $\dot{\gamma}_c$ and what microscopic properties determine its scaling behaviour. To understand this divergence, we have considered the much simpler problem of a single particle undergoing Langevin dynamics in a driven periodic potential. (Independently, a similar model has been used to study stick-slip dynamics in boundary lubrication[22].) In this model, a particle is held at a fixed height above a solid surface which is translating uniformly with speed v. The surface, composed of Lennard–Jones atoms, is analogous to that used in the multi-particle molecular dynamics simulations. As in the collective system, the motion of the particle is independent of the wall velocity at low v and experiences significant slip at high v. The particle achieves pure slip for velocities $v > v_c$. The less corrugated the surface potential, the smaller v_c becomes and the larger the slip at low velocities.

It is natural to assume that the scaling for v_c (or equivalently $\dot{\gamma}_c$)

is set by the liquid–solid interaction timescale, namely $\dot{\gamma}_c^{-1} \sim \tau^{wf} = (m\sigma^{wf^2}/\epsilon^{wf})^{1/2}$. According to this scaling, increasing ρ^w (or likewise decreasing σ^{wf}) should lead to larger values of $\dot{\gamma}_c$. This behaviour is not supported by the data shown in Fig. 2 in which smaller values of σ^{wf} lead to smaller $\dot{\gamma}_c$. We therefore propose a different scaling parameter more closely associated with the surface energy corrugation such that it vanishes in the limit of small ϵ^{wf} and large ρ^w. For both these limits, we expect L_s to increase and $\dot{\gamma}_c \rightarrow 0$. In previous interfacial studies, geometric measures of real surface roughness, like the areal projection of a rough terrain, have been used as a key microscopic parameter controlling slip[4]. We introduce instead a roughness parameter R which characterizes the coarseness of the potential surface, $\phi(\bar{r})$, measured at some fixed height above the wall by a test particle. This potential surface is represented by the vector $x\hat{\mathbf{x}} + y\hat{\mathbf{y}} + \phi^{wf}/\epsilon^{wf}\phi(r)\hat{\mathbf{z}}$. With this definition $R = A/A_\infty - 1$ where $A = \int[1 + (\partial\phi/\partial x)^2 + (\partial\phi/\partial y)^2]^{1/2}\mathrm{d}x\mathrm{d}y$, $A_\infty = \int \mathrm{d}x\mathrm{d}y$, $\phi(\bar{r}) = \Sigma_{N_w} V^{LJ}(|\bar{r} - \bar{r}_i^w|)$, $\bar{r}_i^w$ denotes the position of a wall atom, and $\bar{r}$ locates the test particle.

For the single-particle model just described, v_c scales as $R^{1/2}$ over a wide range of interfacial parameters. This correlation suggests the possibility of describing slip behaviour in terms of a single scalar quantity. But extensions of this analysis to a collective interacting system are complicated by the possibility of layering phenomena at the wall–fluid interface, the dimensionality of the full system, and inertial corrections. Nonetheless, for the limited set of data shown in Fig. 2, we find that $\dot{\gamma}_c$ scales as a power in R with an exponent close to 3/4. Although more studies of this type are required to predict the precise relationship between $\dot{\gamma}_c$ and R, it is possible that a scalar measure of the roughness of the energy surface is a key parameter controlling the amount of slip experienced by a liquid under shear.

Our results indicate that the well-known Navier slip boundary condition is but the low-shear-rate limit of a more generalized universal relationship which is significantly nonlinear and divergent at a critical shear rate, $\dot{\gamma}_c$. The value of $\dot{\gamma}_c$ is set by the corrugation of the potential surface which signals the point at which the solid can no longer impart momentum to the liquid. This means that the same liquid molecules sheared against different substrates will experience varying amounts of slip and vice versa. The functional dependence for L_s shown in Fig. 2a provides a new non-phenomenological boundary condition that can be used to model viscous flows along solid surfaces. This relation provides a mechanism for relieving the well-known stress singularity in spreading liquids and corner flows as it naturally allows for varying degrees of slip on approach to regions of higher shear stress and shear rate. □

Received 23 May; accepted 8 July 1997.

1. Lamb, H. *Hydrodynamics* (Dover, New York, 1932).
2. Batchelor, G. K. *An Introduction to Fluid Dynamics* (Cambridge Univ. Press, 1967).
3. Huh, C. & Scriven, L. E. Hydrodynamic model of steady movement of a solid/liquid/fluid contact line. *J. Colloid. Interface. Sci.* **35,** 85–101 (1971).
4. Hocking, L. M. A moving fluid interface on a rough surface. *J. Fluid Mech.* **76,** 801–817 (1976).
5. Dussan, E. B. On the spreading of liquids on solid surfaces: static and dynamic contact lines. *Annu. Rev. Fluid. Mech.* **11,** 371–400 (1979).
6. Koplik, J., Banavar, J. R. & Willemsen, J. F. Molecular dynamics of Poiseuille flow and moving contact lines. *Phys. Rev. Lett.* **60,** 1282–1285 (1988); Molecular dynamics of fluid flow at solid surfaces. *Phys. Fluids A* **1,** 781–794 (1989).
7. Thompson, P. A. & Robbins, M. O. Simulations of contact line motion: slip and the dynamic contact angle. *Phys. Rev. Lett.* **63,** 766–769 (1989).
8. Thompson, P. A., Brinkerhoff, W. B. & Robbins, M. O. Microscopic studies of static and dynamic contact angles. *J. Adhesion Sci. Technol.* **7,** 535–554 (1993).
9. Moffatt, H. K. Viscous and resistive eddies near a sharp corner. *J. Fluid Mech.* **18,** 1–18 (1964).
10. Koplik, J. & Banavar, J. R. Corner flow in the sliding plate problem. *Phys. Fluids* **7,** 3118–3125 (1995).
11. Pearson, J. R. A. & Petrie, C. J. S. in *Polymer Systems: Deformation and Flow* (eds Wetton, R. E. & Whorlow, R. W.) 163–187 (Macmillian, London, 1968).
12. Richardson, S. On the no-slip boundary condition. *J. Fluid Mech.* **59,** 707–719 (1973).
13. Denn, L. M. Issues in viscoelastic fluid mechanics. *Annu. Rev. Fluid Mech.* **22,** 13–34 (1990).
14. Durbin, P. A. Considerations on the moving contact-line singularity, with application to frictional drag on a slender drop. *J. Fluid Mech.* **197,** 157–169 (1988).
15. Koplik, J. & Banavar, J. R. Continuum deductions from molecular hydrodynamics. *Annu. Rev. Fluid Mech.* **27,** 257–292 (1995).
16. Thompson, P. A. & Robbins, M. O. Shear flow near solids: epitaxial order and flow boundary conditions. *Phys. Rev. A* **41,** 6830–6837 (1990).
17. Thompson, P. A. & Robbins, M. O. The origin of stick-slip motion in boundary lubrication. *Science* **250,** 792–794 (1990).
18. Stevens, M. J. *et al.* Comparison of shear flow of hexadecane in a confined geometry and in bulk. *J. Chem. Phys.* **106,** 7303–7314 (1997).
19. Allen, M. & Tildesley, D. *Computer Simulation of Liquids* (Clarendon, Oxford, 1987).
20. Loose, W. & Hess, S. Rheology of dense fluids via nonequilibrium molecular hydrodynamics: shear thinning and ordering transition. *Rheol. Acta.* **28,** 91–101 (1989).
21. Atwood, B. T. & Schowalter, W. R. Measurements of slip at the wall during flow of high-density polyethylene through a rectangular conduit. *Rheol. Acta.* **28,** 134–146 (1989).
22. Rozman, M. G., Urbakh, M. & Klafter, J. Stick-slip motion and force fluctuations in a driven two-wave potential. *Phys. Rev. Lett.* **77,** 683–686 (1996).

Acknowledgements. P.A.T. thanks the Exxon Education Foundation and an NSF CAREER award which helped initiate these studies. S.M.T. was supported by the Exxon Education Foundation and the NSF through a Research Initiation and CAREER award, and a seed grant from the MRSEC program of the Princeton Materials Institute.

Correspondence should be addressed to S.M.T. (e-mail: stroian@princeton.edu).

Laser action in organic semiconductor waveguide and double-heterostructure devices

V. G. Kozlov, V. Bulović, P. E. Burrows & S. R. Forrest

Center for Photonics and Optoelectronic Materials, Department of Electrical Engineering and the Princeton Material Institute, Princeton University, Princeton, New Jersey 08544, USA

Stimulated emission by optical pumping of solid-state organic materials has been well known since the late 1960s following the first demonstrations of laser action in dye-doped gels and molecular crystals[1–4]. Interest in this field has been revived by the demonstration of efficient, long-lived and intense electroluminescence in both polymeric[5] and small-molecular-weight[6] organic thin films, which indicates the possibility of laser action in these materials. Several recent studies of optically pumped polymers have reported emission phenomena suggestive of laser action[7–9]. Here we present clear evidence for laser action from optically pumped, vacuum-deposited thin films of organic molecules, in both slab-waveguide and double-heterostructure configurations. This realization of laser action in conducting organic thin films should open the way to the development of a new class of electrically pumped laser diodes.

Lasing (in contrast to amplified spontaneous emission, superluminescence or related phenomena) can be unambiguously identified from five phenomena: (1) a clear indication of a threshold in output energy as a function of input (or pump) energy, with a high lasing efficiency above threshold; (2) strong output beam polarization; (3) spatial coherence (as indicated by a diffraction-limited output beam or speckle); (4) significant spectral line narrowing; and (5) the existence of laser cavity resonances, or modes. Although several recent reports[7–9] on polymer-based optically pumped thin films have discussed structures showing one or two of the above phenomena, there has (to our knowledge) been no report of all of these properties having been observed in such a system.

Tris-(8-hydroxyquinoline) aluminum (Alq_3) doped with 2.5% DCM laser dye provides an excellent laser material[10] as the red stimulated emission of DCM at a wavelength of $\lambda = 645$ nm is far from the ultraviolet absorption edge of the Alq_3 host (at $\lambda = 450$ nm)[11], whereas the absorbance of the DCM is centred near the emission maximum of Alq_3 (at $\lambda = 530$ nm), thereby providing for efficient Förster energy transfer[12] from ultraviolet-excited Alq_3 (see Fig. 1 for molecular structural formulae of Alq_3 and DCM). Doping also allows for reduction of the density of the optically active DCM molecules (thereby reducing the effective density of states), which lowers the threshold and increases the efficiency of a laser[13]. In fact, efficient orange electroluminescence for DCM-doped Alq_3 films has been demonstrated[6].

Lasers shown in Fig. 1 were grown on InP substrates pre-coated